Int. J. Electrochem. Sci., 11 **(2016)** 3467 - 3491

International Journal of
ELECTROCHEMICAL
SCIENCE
www.electrochemsci.org

Development of Novel Phosphorylated Cellulose Acetate Polyelectrolyte Membranes for Direct Methanol Fuel Cell Application

M. S. Mohy Eldin[1,2,*], *M. H. Abd Elmageed*[3], *A. M. Omer*[2], *T. M. Tamer*[2], *M. E. Yossuf*[4], *R. E. Khalifa*[2]

[1] Chemistry Department, Faculty of Science, University of Jeddah, Asfan, P. O. Box: 80203, Jeddah 21589, Saudi Arabia
[2] Polymer Materials Research Department, Advanced Technology and New Materials Research Institute, MuCSAT, New Borg El-Arab City 21934, Alexandria, Egypt
[3] Chemical Engineering Department, Faculty of Engineering, Alexandria University, Alexandria, Egypt.
[4] Computer-Based Engineering Applications Department, Informatics Research Institute, MuCSAT, New Borg El-Arab City 21934, Alexandria, Egypt
[*]E-mail: m.mohyeldin@mucsat.sci.eg

Received: 25 December 2015 / *Accepted:* 9 March 2016 / *Published:* 1 April 2016

A novel phosphorylated cellulose acetate membranes (PCA) was prepared using epichlorohydrin as an activating agent and evaluated as a potential polyelectrolyte membrane for DMFC applications. The PCA membranes exhibit higher water uptake, low methanol uptake. Thermal oxidation stability, TGA, and tensile characterization impelled good thermomechanical stability than the native CA membranes. Furthermore, the PCA membranes are found to have a low methanol permeability ($2.4*10^{-15}$ Cm^2/S) which much smaller than that of Nafion membranes ($1.14*10^{-9}$ Cm^2/S).The basic manufacture technology and cheapness of CA polymer recommend this candidate for fuel cells application. In conclusion, the formulated PCA membranes can be applied as new polyelectrolyte membranes for the DMFCs application.

Keywords: Activation; Phosphorization; Cellulose acetate membrane; Fuel cell; Ions exchange capacity, polyelectrolyte membranes.

1. INTRODUCTION

Recently, much attention to the conversion devices such as fuel cells particularly for automotive and stationary power [1-4] applications has gained much interest, due to the further

doi: 10.20964/110318

increase in the world population resulting in increasing energy consumption. In addition to the worldwide concern about environmental problems caused by the daily use of fossil fuel in the electricity production [5].Thus successful development proton exchange membranes (PEM) has received much attention as an efficient solution for chemical energy transformation into electric power and dramatically reductions of harmful pollutants as the overall emissions from a fuel cell vehicle are 90% less than from conventional vehicles [6, 7]. A fuel cell must successfully allow the free movement of protons across its structure, thus, researchers focus on cation exchange membranes that have fixed anionic charges permits easy proton transport [8]. Direct methanol fuel cells (DMFCs) which use methanol as fuel regarded as a promising candidate for their high potential in a stationary application, transportation (electric vehicles) and portable power sources such as cellular phones, and laptops [9] due to the easily transportation, storage and distribution of the fuel. However, the commercial of DMFC has been limited by numerous valuable objects. A slow kinetics of the methanol oxidation reaction in addition to its crossover to cathode side through Polymer electrolyte membrane parallel with the low electrocatalytic activity of the Pt catalyst caused by the adsorption of CO impurities formed during methanol dehydrogenation at the catalysts surface [10] are the main challenges. Perfluorosulfonate Ionomer Membranes such as such as NafionTM (DuPont), AciplexTM (Asahi) and DowTM (Dow) [11] has widely used as the primary proton conducting polymer electrolyte membrane for DMFC application. Besides their excellent chemical, mechanical, thermal stability and high proton conductivity (~0.1 Scm^{-1}), Nafion membranes have drawbacks. High cost, methanol crossover that resulted in fuel not only loose but also decreases electrochemical performance because of mixed potential at the cathode caused by the methanol oxidation at the cathode and conductivity loss at elevated temperatures higher than $100^{o}C$ [12,13]. Therefore, researchers focus on dealing with these problems through different strategies including the modification of Nafion membranes i.e. preparing Nafion/polymer composites (e.g. polybenzimidazole [14], polyaniline [15], poly(-POSS) [16]) and Nafion/inorganic particles nanocomposites(e.g. montmorillonite [17], zirconium phosphate [18], silicon oxide [19]) membranes. On the other hand; there are many works have been conducted in investigating the substitutive membranes for the perfluorinated membranes by seeking not by first looking for high proton conductivity, but by first seeking substantial methanol barriers. Natural and synthetic polymers such as PVA, PVC, PVDF, FEP, PFA and cross-linked PTFE [20, 21] intensively investigated lately as promising base polymer electrolytes for DMFCs [22, 23, 24]. Development of Polymer electrolytes from renewable sources is becoming a promising substitute for synthetic ones as there are cheap and environmentally friendly [25]. Among these, natural polymer is alginate and polysaccharides such as chitosan as a derivative of low cost and naturally abundant chitin [26, 27]. In this study, for the first time, novel polyelectrolyte membranes based on CA structure were synthesized, and the essential characters for future DMFC applications performed. Firstly, the activation process was carried out using Epichlorohydrin (ECH) followed by introducing phosphoric acid group through phosphorization processes.The impact of different modification and activation conditions on the activation and phosphorization process was explored to find the best conditions. The prepared membranes then physicochemically characterized. Water and methanol uptake, dimensions changes, tensile strength (TS), ions exchange capacity (IEC) and methanol permeability conducted. Furthermore, FTIR, XRD, and TGA analysis provided to prove the occurrence of the phosphorization

process while SEM analysis examined the homogeneity of the formed phosphorylated membranes. Furthermore, optical properties, Wettability, and finally thermal oxidation stability performed.

2. EXPERIMENTAL

2.1. Materials

Cellulose acetate (Degree of acetylation 40%) and Epichlorohydrin (purity 99.5%) supplied by Sigma- Aldrich Chemie Gmbh. (USA). Orthophosphoric acid (purity 85% extra pure) and Acetone (purity 90%) supplied by Sigma- Aldrich Chemicals Ltd. (Germany). Methanol (purity 99.8%) supplied by Fluka Chemie GmbH. (Switzerland). Hydrochloric acid (purity 37%) provided by POLSKIA ODCZYNNIKI CHIMICZNE S.A. (Finland). Sodium Chloride, Sodium Hydroxide, Hydrogen Peroxide, Phenol phethalin, and Ethyl alcohol (absolute) are analytical grade supplied by El-Gomhouria Co. (Egypt).

2.2. Methods

2.2.1. Membrane preparation

Activation process

Cellulose acetate powder (CA) dissolved in acetone followed by the addition of ECH in different molar ratios; 1:1, 1: 2, 1: 3, 1: 4 and 1: 5. The activation process conducted at various temperatures (35–65°C) for different time periods (2–14h) using a water bath. The activation containers left at R.T for 5h and then in a water bath for 7h. After completion of the activation process, the solution was casting in a Petri dish and allowed to dry at 40°C. The prepared membranes epoxy content measuring as follows:

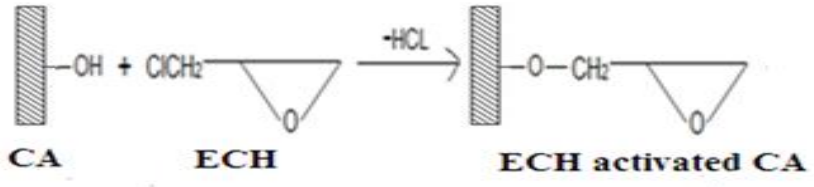

Scheme 1. Reaction of CA with ECH.

Epoxy content determination

The epoxy content of ECH activated CA membranes measured according to the published method [28] using simple back titration procedure. Briefly, the activated samples were soaked in 50ml. 0.1M HCl solutions at room temperature for at least 12h with shaking. The HCl molecules are reacted to hydrolysis the epoxy ring of ECH. The left HCl molecules titrated with 0.1M NaOH. The epoxy

content correlated to the volume of HCl consumed in opening the epoxy ring as shown in the following equation:

$$X = \frac{(v_1 - v_2)N}{g} \quad (1)$$

Where, X: mg equivalent of ECH per g of sample, V_1: Volume of NaOH in the original sample, V_2: Volume of NaOH in the modified sample, N: Normality of NaOH, g: Weight of the sample tested.

Phosphorization process

Activated CA solution reacted with different orthophosphoric acid solution concentrations (0.25- 2 molar ratios of OPA); Scheme 2. The reaction conducted at temperatures range (25–65°C) in a water bath at various time periods (2–10h). After completing the reaction, the modified solution was casted and dried. Unreacted, excess OPA removed through successive washing with distilled water.

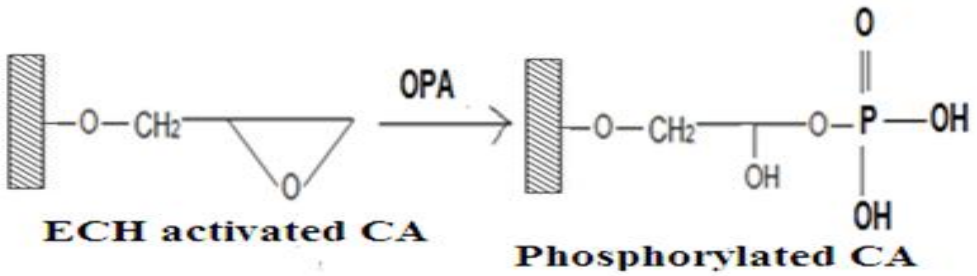

Scheme 2. Reaction of ECH activated CA with OPA.

2.2.2. Membrane characterization

Water and methanol uptake

Water and methanol uptake calculated by soaking the membranes in water or in methanol, which placed in a closed glass container at ambient temperature overnight. After that, the swollen membranes removed, and the excess of adhered water or methanol on the surface removed using tissue paper, then weighed. The liquid uptake (water or methanol) estimated using the following equation [29]:

$$LU(\%) = \frac{W_w - W_d}{W_d} \times 100 \quad (2)$$

Where: W_d is the dry and W_w is the wet weights of membrane samples.

Dimensional change

The Impact of deionized water or methanol on the membranes dimensions determined by soaking the membranes in the mentioned solvents [30, 31] at room temperature for 24h. According to the following equation, the membrane's area change percentage (ΔA %) calculated:

$$\Delta A\% = \frac{A - A_o}{A_o} \times 100 \qquad (3)$$

Where: A_0 is the dry membrane, and A is the wet membrane areas.

Infrared spectrophotometric analysis (FTIR)

Changes resulted from the activation and modification of the CA membranes have been followed by monitoring the characteristic functional groups using Fourier transform infrared spectrophotometer (Shimadzu FTIR-8400 S), Japan.

Thermal gravimetric analysis (TGA)

Thermal changes of activated and modified CA membranes traced using thermogravimetric analyzer (Shimadzu TGA-50, Japan).

Scanning electron microscopic analysis (SEM)

Morphological changes of the membranes surface were followed using energy-dispersive analysis X-ray (Joel Jsm 6360LA), Japan.

X-Ray diffraction analysis (XRD)

X-ray patterns of the Virgin CA, activated CA and phosphorylated CA membranes obtained using diffractometer (Schimadzu7000).

Surface roughness

The surface roughness of all prepared membranes was measured using surface roughness tester (SJ- 201P), Japan. Onto a glass slide with a double-sided tap, the samples mounted. Minimum sample dimensions were 4cm×5cm. All results are the average of six measurements.

Thermal oxidative stability

Membrane strips (2cm×2cm) immersed in Fenton's reagent (4ppm $FeSO_4$ in 3%H_2O_2) and kept at 80°C under stirring. The weight loss of the membrane strips followed at fixed time intervals along selected period. The Fenton's reagent changed every 10h [32].

Optical properties (Colorimeter)

The change color values for different sites of membranes were measured using a colorimeter. Films color was measured by an X-Rite (Model Sp64; Made in the USA). The colorimeter calibrated with white and black plates. A white standard color plate for the instrument calibration was used as a background for color measurements of the films. The system provides the values of three color components; L* (black-white component, luminosity), and the Chromatics coordinates, a* (+red to −green component) and b* (+yellow to −blue component) [33]. Color differences ΔE* were also calculated by the following equation:

$$\Delta E = \sqrt{\left(\Delta L^*\right)^2 + \left(\Delta a^*\right)^2 + \left(\Delta b^*\right)^2} \qquad (4)$$

Where: $\Delta L^* = L^* - L_0^*$, $\Delta a^* = a^* - a_0^*$, $\Delta b^* = b^* - b_0^*$ being: L_0^*, a_0^*, b_0^* are the color parameter values of the standard and L^*; a^*; b^* the color parameter values of the sample.

2.2.3. Ion exchange capacity

The ion exchange capacity (IEC) of the phosphorylated membranes was determined using acid-base titration [34]. Weighed samples placed in 20cm^3 of a 2M NaCl solution for at least 12h, and then the solution titrated with a NaOH solution of known concentration. IEC calculated as follows:

$$IEC(m_{eq}/g) = \frac{V_{NaOH} \times C_{NaOH}}{W_d} \qquad (5)$$

Where: V, C, and W_d are the volume of NaOH consumed in titration, the concentration of NaOH solution, and the weight of the dry membrane sample, respectively.

Methanol permeability measurements

A home-made glass diffusion cell [35] was used to measure the Methanol permeability. The cell consist of two compartments namely (compartment A) which filled with 2M methanol aqueous solution and (compartment B) which contain distilled water each with a volume of 100ml. The membrane under test was located at the center of the cell as showed in Figure1. With continuous stirring to keep uniform concentration during the experiments and each membrane was soaked in a 2M methanol solution for at least 24h, before testing the sample solution (500μL) withdrawn from the water compartment using a micro-syringe periodically each 25min for 2h and the methanol concentration was measured using HPLC analyzer. All measurements will be carried out at 25°C. The concentration of methanol in water compartment is related to time by the following equation:

$$C_B(t) = \frac{A \times P}{V_B \times L} C_A\left(t - t_o\right) \qquad (6)$$

Where P is the methanol permeability, which defined as the product of methanol diffusion coefficient (D) through the membrane and the partition coefficient (K), i.e., (P = DK). C_B is the

concentration of methanol in the water compartment (B) at time t. C_A is the initial concentration of methanol in the compartment (A). A is the membrane working area. L is the membrane thickness. V_B is the volume of water compartment. "t" is the time lag, that linked with the methanol diffusion coefficient (D) according to the following formula: ($t_o = L^2/ 6D$). The methanol permeability (P) obtained from the slope of the linear relationship between the concentration of methanol in the water compartment (C_B) and the time (t) according to the following equation:

$$P = \alpha \frac{V_B}{A} \times \frac{L}{C_A} \qquad (7)$$

Where α is the slope of the linear function of C_B versus t.

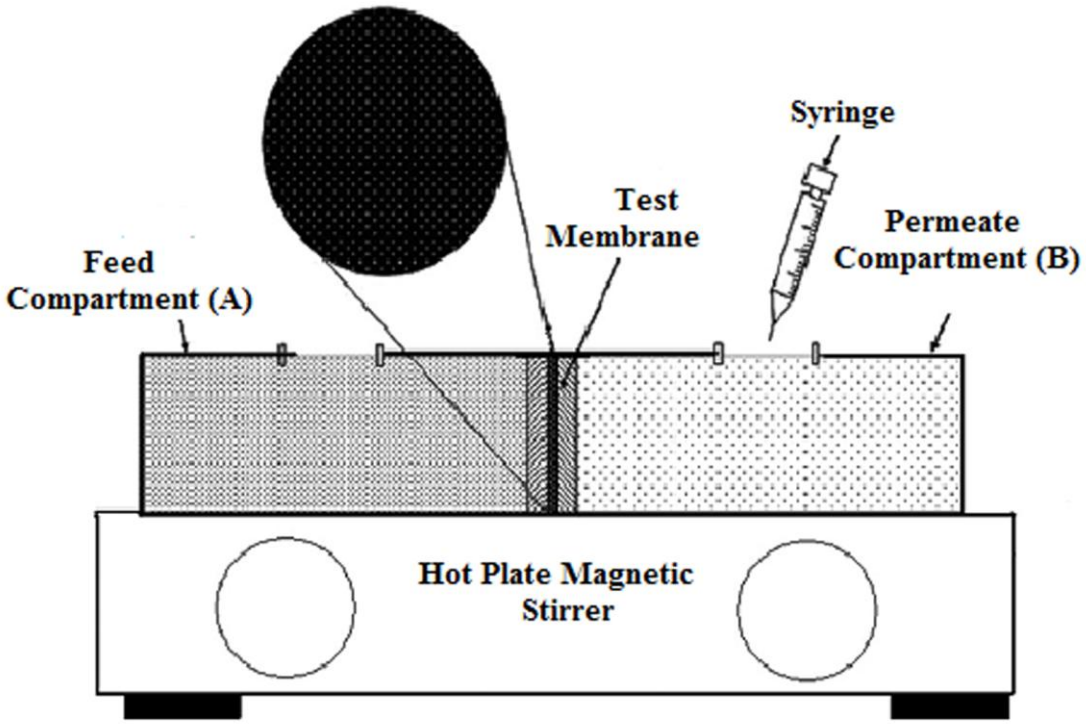

Figure 1. Glass diffusion cell for methanol crossover measurements.

Tensile strength

Tensile strength (TS) is a measure of the resistance of original CA and its modified forms to the direct tension. TS defined as the force required breaking a strip of the sample, which has a specified length and a width of 15mm using LLOYD Instruments LR 10 K.

Breaking length (*m*) = TS (kg) strip length (*m*)/ strip weight (kg).

1 kg/15 mm = 3.73 lb/in.

Zero-span breaking length ¼ kg breaking load 200,000/ [basis weight/sq in*3].

The sample size is (1.5-5) cm.

The mean values of three measurements for each sample reported.

3. RESULTS AND DISCUSSION

3.1. Activation process

The influence of different factors namely; ECH concentration, reaction time, reaction temperature and pH on the activation process studied. The results discussed in details and the activation process reaction presented in Scheme 1.

3.1.1. Effect of ECH concentration

The impact of variation of the ECH concentration on the epoxy content investigated. Figure 2 shows that the increment of the ECH concentration from 1: 0.5 to 1: 5 molar ratios for (CA: ECH), clearly increased the epoxy content of the activated membranes. The maximum epoxy content obtained at 1:3 molar ratios. Beyond this ratio, no significant improvement in the epoxy content observed.These observations may attribute to that increasing of the ECH concentration facilitates its diffusibility toward the cellulosic chains [36]. This behavior may simply attribute to the formation of epoxy group's results from the reaction of the ECH's chlorine atom with the hydroxyl group of CA, which represents active sites for functionalizations step using orthophosphoric acid.

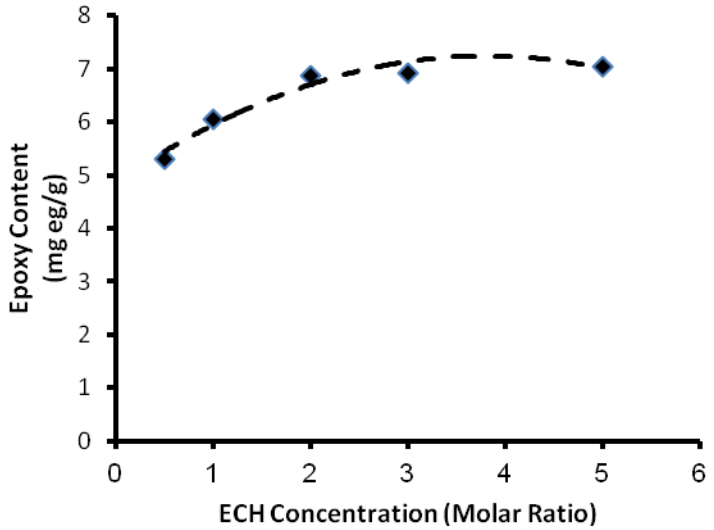

Figure 2. Effect of variation of the ECH concentration on the epoxy content (55°C for 12h).

3.1.2. Effect of activation temperature

Figure 3 shows the impact of varied the reaction temperature with ECH on activation process. The figure revealed that there is a progressive increment of the epoxy content with an elevation of the reaction temperature from 35 to 55°C. The maximum epoxy content observed of 55°C. Further elevation of the reaction temperature has no effect. The improvement of the reaction rate as a result of increasing the reaction temperature related to increasing the diffusion of ECH into the CA matrix. That

consequently improved the membranes hydrophobicity. Prolongation of the reaction time to 12h at a high temperature (> 55C^{o}) on the epoxy contents has a neglectable effect [36].

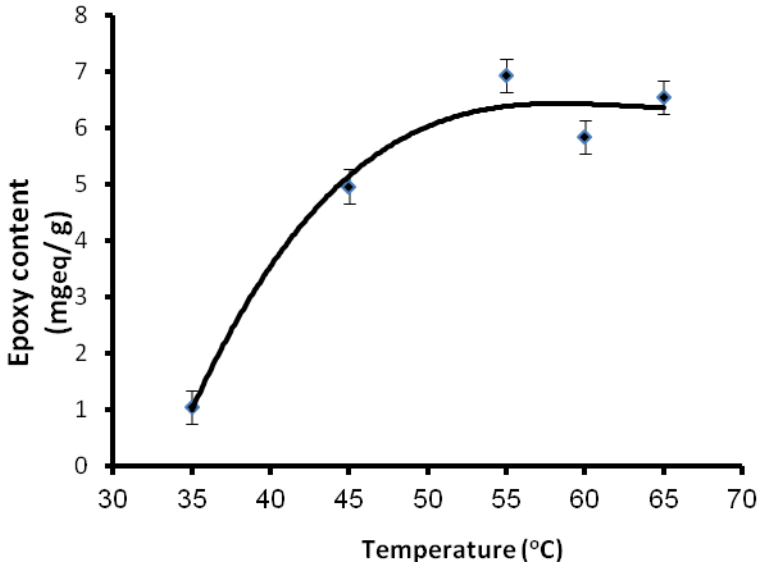

Figure 3. Effect of variation of the activation temperature on the epoxy content (1:3 molar ratio of CA: ECH at 12h and pH8).

3.1.3. Effect of activation time

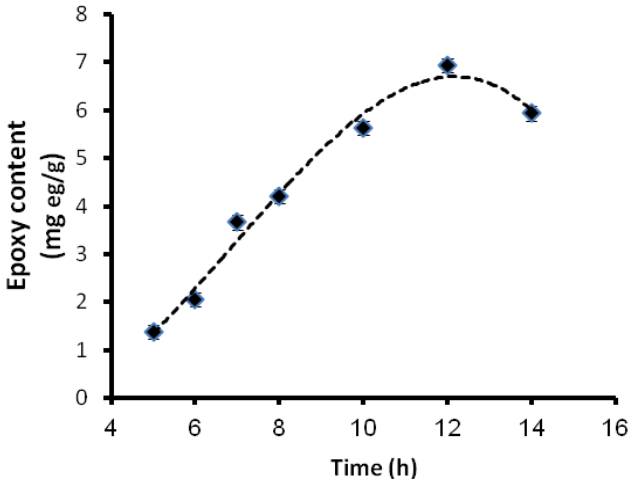

Figure 4. Effect of variation of the activation time on the epoxy content (1:3 molar ratio of CA: ECH 55°C and pH8)**.**

The influence of variation the reaction time on the activation process illustrated in Figure 4. The results reveal that increasing the time from 5 to 14h increased epoxy contents to reach maximum values at 12h this kind of behavior is due to that increasing time of activation will increase the number of activated hydroxyl groups on the CA chains. On the other hand, further increases in the reaction

time to 14h have no significant effect on the epoxy contents due to the formation of a diffusion barrier with a hydrophobic nature against ECH diffusion into CA chains.

3.1.4. Effect of activation pH

The impact of various pH values studied for the activated CA membranes as shown in Figure 5. Data indicated that the epoxy contents increased by increasing the pH value to reach a maximum value at pH8. A decrease in the epoxy content observed with further increase in reaction's pH. That was expected behavior because etherification and reactions involving epoxides could be accomplished in an alkaline medium [37] and the reactions rate easily controlled.

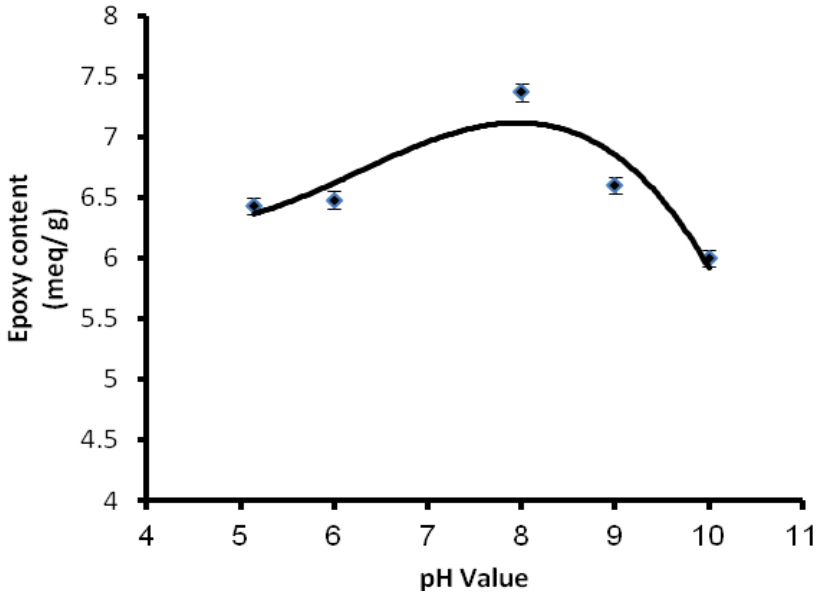

Figure 5. Effect of variation of the reaction's pH values on the epoxy content (1:3 molar ratio of CA: ECH at 12h at 55°C).

3.2. Phosphorization process

3.2.1. Effect of OPA concentration

Ionic conductivity is known to be correlated directly to the ions exchange capacity of the membranes. Figure 6 indicates that the IEC of phosphorylated CA membranes increased exponentially with increasing of OPA concentration, and the highest IEC obtained using 2M OPA [38]. Increasing OPA concentration creates high concentration gradient between the CA membrane solid phase and OPA liquid phase. That leads to increasing the diffusion of OPA into the CA bulk matrix and consequently producing more ionizing sites responsible for the IEC.

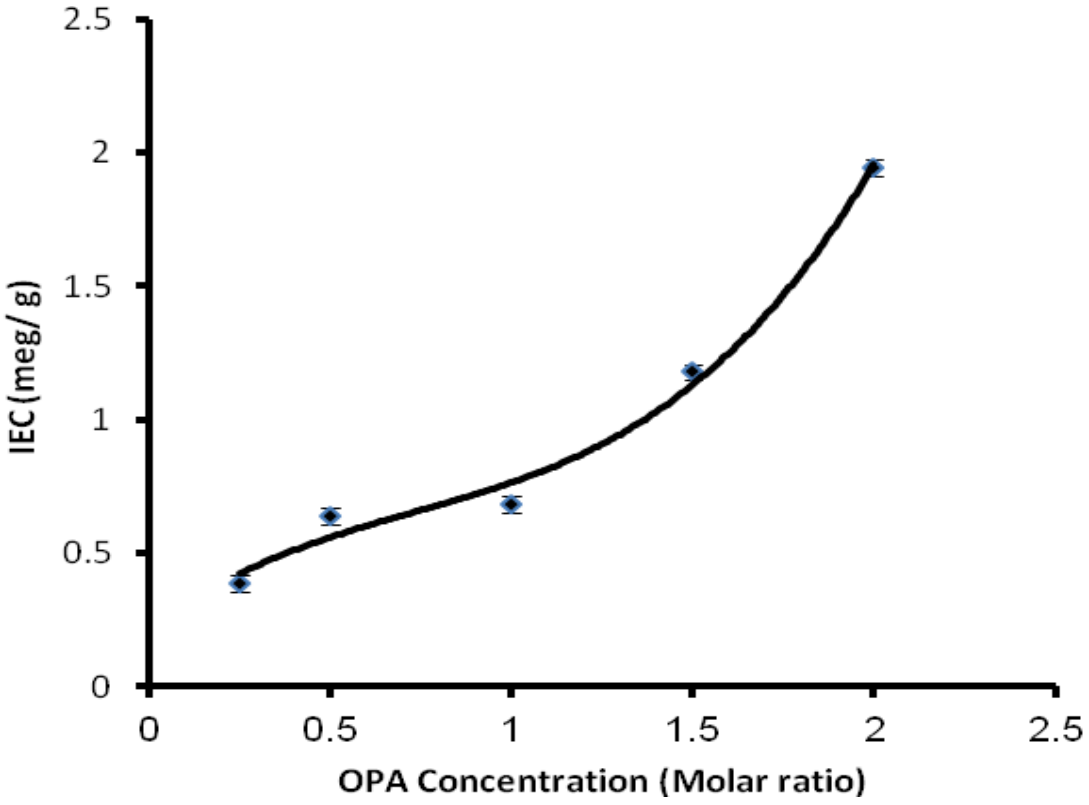

Figure 6. Effect of orthophosphoric acid concentration on the ion exchange capacity at 35°C and 10h.

3.2.2. Effect of reaction temperature

The influence of elevating of the reaction temperature on the producing ionizing exchangeable sites is shown in Figure7. No significant changes of the IEC observed within the studied range of the reaction temperature; 25-65°C. An explanation could give according to the hydrophilic nature of phosphoric groups that attached to the epoxy groups easily in addition to suitable reaction time. Carry out the reaction in one phase limited the effect of the reaction temperature [39].

3.2.3. Effect of the reaction time

Figure 8 impelled the impact of prolongation of the reaction time on the IEC of the activated CA membranes. The progressive increment of the IEC observed, and maximum values reached after 8h, then leveled off. That behavior expected due to increasing the reaction between epoxy groups of attached ECH and the orthophosphoric acid molecules producing higher ions exchange capacity character [36].

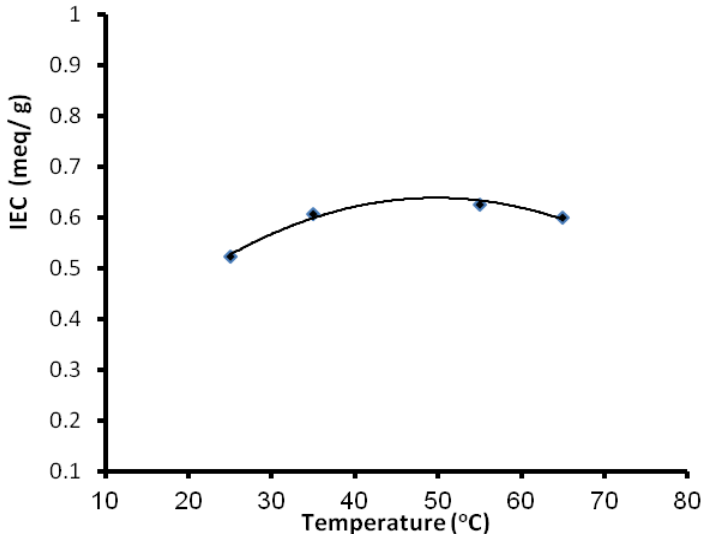

Figure 7. Effect of variation of the reaction's temperature on the ions exchange capacity (CA: ECH: OPA; 1: 3: 0.5 for 8h).

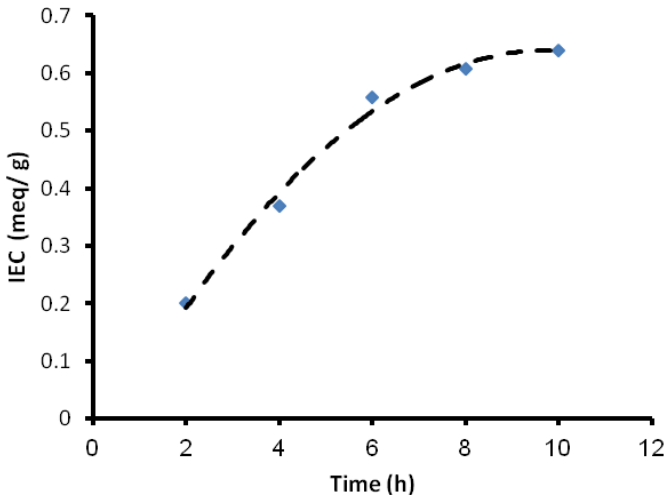

Figure 8. Effect of variation of the reaction's time on the ions exchange capacity (CA: ECH: OPA; 1: 3: 0.5 at 35°C).

3.3. Membrane characterization

3.3.1. Water and methanol uptake

The ionic nature of water molecules determined to a great extent the mobility of the H^+ ions and consequently affects the proton conductivity of the polyelectrolyte polymeric membranes in fuel cells essentially. Accordingly, a direct relation established between the water absorption and the ionic conductivity. The water and methanol uptake of the phosphorylated CA membrane at a different concentration of OPA and different phosphorylated time recorded in Figure 9.

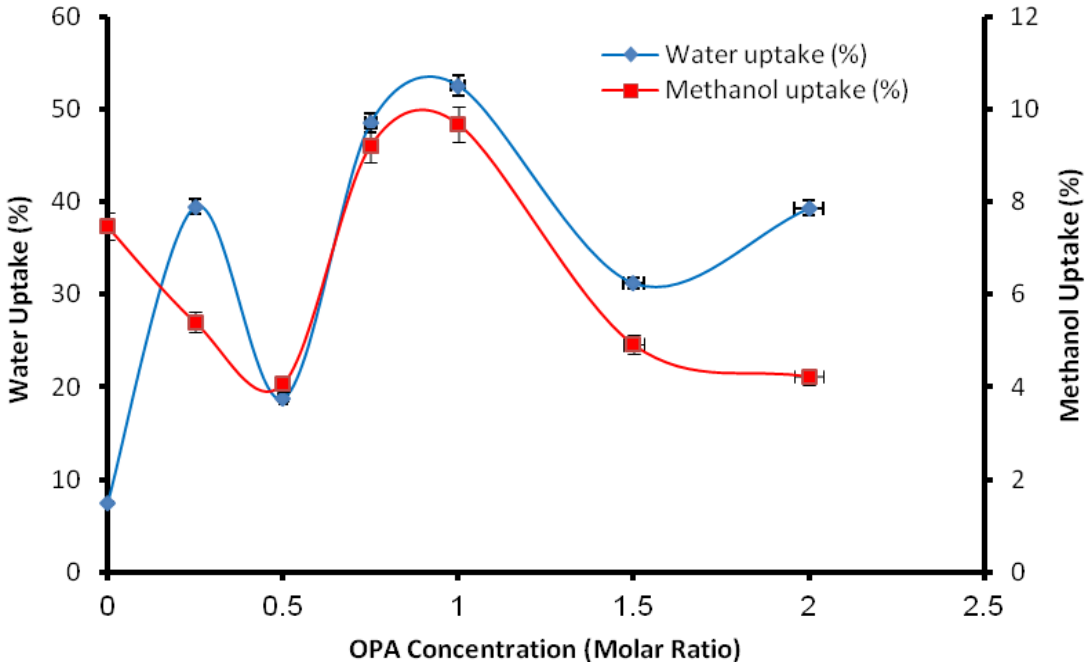

Figure 9a. Water and methanol uptake of phosphorylated CA membranes at various molar ratios of OPA at 8h, 35°C.

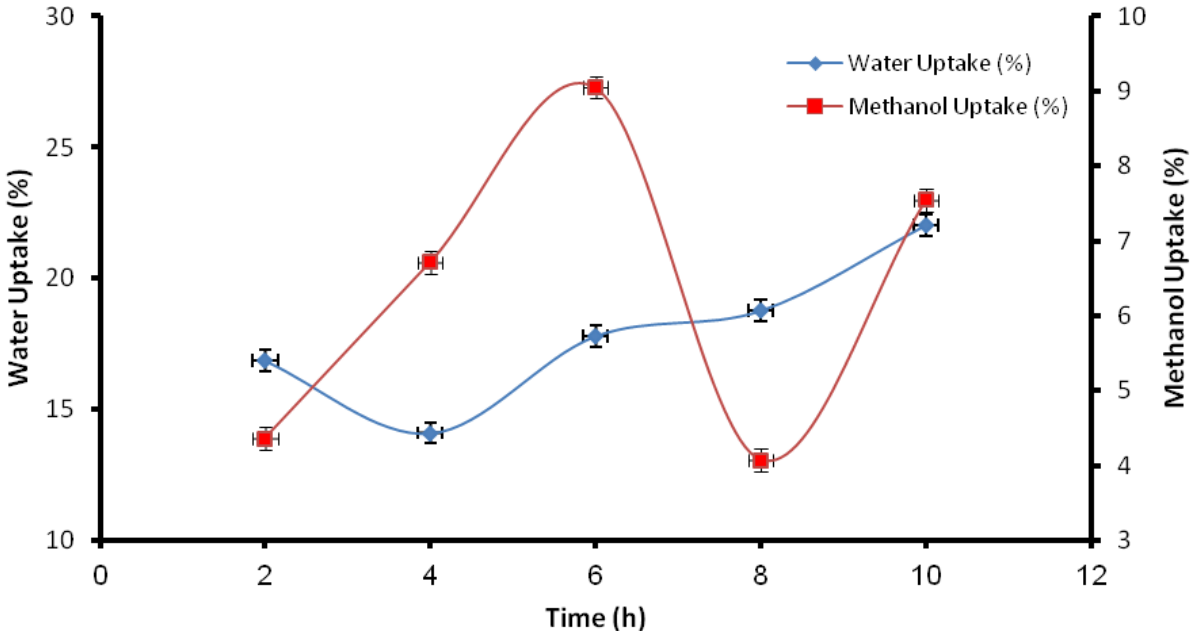

Figure 9b. Water and methanol uptake of phosphorylated CA membranes at 35°C and molar ratio 1: 0.5 of CA and OPA respectively at different time intervals.

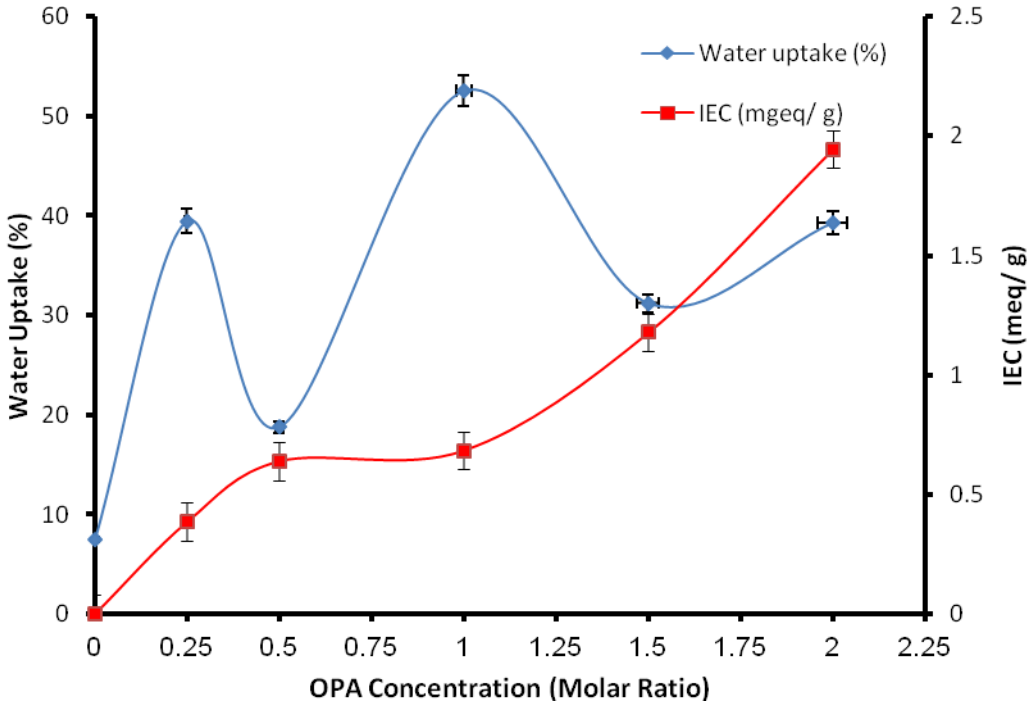

Figure 10. The water uptake and the IEC behavior of the phosphorylated CA membranes at various molar ratios of OPA (8h, and 35°C).

From data obtained it was obvious the positive effect of modification process on water sorption of the modified membranes compared with the original and activated ones obtained by increasing the reaction time for the same OPA concentration. That may refer to the increment of the membrane hydrophilicity induced by the phosphoric groups [36]. It can reveal that the membranes water uptake could be controlled and varied by changing the preparation conditions. On the other hand, the methanol uptake for all phosphorylated membranes was decreased. Formation of hydrogen bonding between the methanol molecules and the ionic sites over the membrane backbone could explain the observed behavior.

Figure 10 shows an increasing trend of the IEC and the water uptake values with increasing of the OPA concentration. The water uptake varied from 7.47 to 52.52% for activated and phosphorylated CA membranes, while the IEC values ranged from 0.38 to1.195 meq/g as the phosphorization level increased from 0.25 to 2%. Furthermore, a similar trend of gradual increment of both the water uptake and the IEC of the phosphorylated membranes observed. That could attribute to the introduced phosphoric acid hydrophilic groups. Compared with Nafion®117 membranes, the water uptake of the phosphorylated membrane is lower while it has an almost same value of IEC [40].

3.3.2. Dimensional changes

Following the changes in dimensions of the modified membranes at different reaction time after their swelling in water and/or methanol for 24h presented in Table 1. Inspecting the results

indicate the significant changes in the modified membranes dimensional during the swelling process regarding the original and activated membranes. That confirmed the subjected of the activated membranes to dimensional changes as a result of the modification process.

Table 1. Dimensional change of the phosphorylated CA membranes at 35°C and molar ratio 1: 3: 0.5 of CA: ECH: OPA respectively, at different time intervals

Phosphorization time (h)	Dimension changes In Water %	Dimension changes In Methanol %
2	15.5	10.25
4	10.25	15.5
6	15.5	5
8	10.25	5
10	10.25	10.25

3.3.3. Mechanical characteristics

A positively impact of the force on the elongation of the membrane was the observed result as shown in Table 2, where the elongation of the membrane increased as a consequence of the phosphorization. That means, after the phosphorization, modified membranes became more elastic than the original and activated ones. In general, an improvement of the mechanical properties of phosphorylated membranes has been obtained.

3.3.4. Infrared spectrophotometric analysis

Analysis of FTIR spectroscopic investing structures for original, activated and phosphorylated CA membranes was carried out using Fourier Transform Infrared Spectrophotometer (Shimadzu FTIR - 8400 S, Japan) as shown in Figure 11.The recognize of the characteristic absorption band of OH at 3498.99, 3489.34 and 3373.61cm^{-1} for original, activated and phosphorylated membranes.With the addition of OPA, a very broad absorption band appears in the wave number at 2918cm^{-1}. The change of T% at around 34980- 3414cm^{-1}, the particular band for OH groups of CA, indicates the consumption of some OH groups at the activation process with ECH. Activation of CA is a possibility here depends on the activation conditions and the number of activated OH groups relative to the ECH concentration used during the activation step. Similar results observed by other authors during activation of carboxymethyl cellulose (CMC) with ECH for preparing ion exchangers [41].These figures clearly indicate the effect of the activation and phosphorization process on CA backbone structure.

Table 2. Mechanical properties of the phosphorylated CA membranes at 35°C and molar ratio 1: 3: 0.5 as CA: ECH: OPA respectively, at different time intervals

Phosphorization time (h)	Tensile Strength (N)	Elongation (mm)
Original CA membrane	15.21	2.645
Activated CA	45.45	7.75
Phosphorylated CA (2hr)	34.5833	9.4825
4	34.9702	8.0550
6	28.9522	9.0650
8	37.7171	8.2600
10	24.7192	6.7860

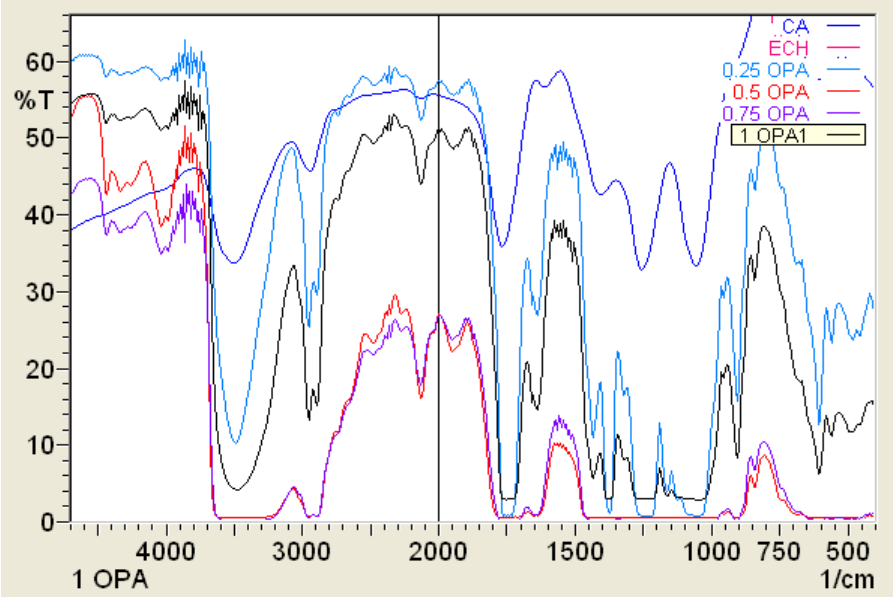

Figure 11. FTIR spectra of original CA, activated CA, and phosphorylated CA membranes.

3.3.5. Thermal gravimetric analysis (TGA)

Thermal gravimetric analysis of the original CA, activated CA, and phosphorylated CA membranes performed using TGA analyzer at nitrogen atmosphere with a heating rate of 20°C/min. It is clear from Figure12 and Table 3 that there are three thermal decomposition steps. Adsorbed water evaporation up to 200°C presents the first weight loss. The second decomposition step of the phosphonic acid groups appears between 280 and 400°C. Finally, at a temperature higher than 400°C, the backbone glucose degradation appears.

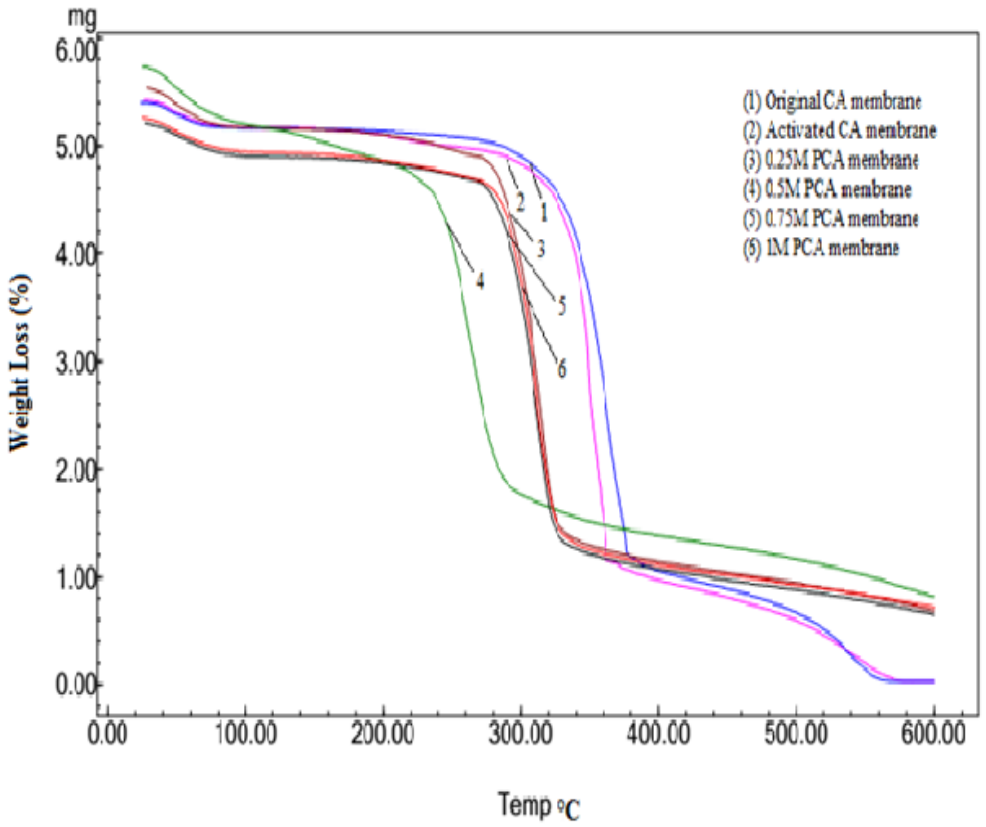

Figure 12. TGA thermograph of the native CA membranes, activated CA membranes and PCA membranes.

Table 3. TGA analysis for the original, activated and PCA membranes

Membrane with molar ratio	$T_{1/5}$	Weight loss (%) at ambient temperature (0-150°C)
Original CA membrane	360.83	4.611
Activated CA (1:3)	350.23	4.75
PCA (O.25M)	328	5.59
PCA (0.5M)	334.45	5.31
PCA (0.75M)	336.67	4.67
PCA (1M)	339.09	3.97

The above indicates the suitability of the prepared membranes to work in low-temperature fuel cells; temperature less than 200°C. It also noticed that 50% weight loss in case of the original membranes observed at 360°C. A relatively high rate of weight loss observed above 280°C. Above

360°C, the rate of weight loss becomes lower, and the percent loss at ambient temperature was found to be 4.61, 4.75, and 5.31 for original, activated and phosphorylated membranes. That is expected behavior as the phosphorylated membranes became thermally unstable at elevated temperature giving an indication for the formation of a new chemical structure different from original CA one.

3.3.6. Morphological characterization (SEM)

Figure 13 displays SEM pictures (Surface and cross-section) for CA, activated CA and phosphorylated CA with different concentrations. Obvious differences of the morphological structure of the phosphorylated CA membranes than both the original CA and the activated CA membranes observed. That proved that the changes in the PCA membranes structured result of the phosphorization process.

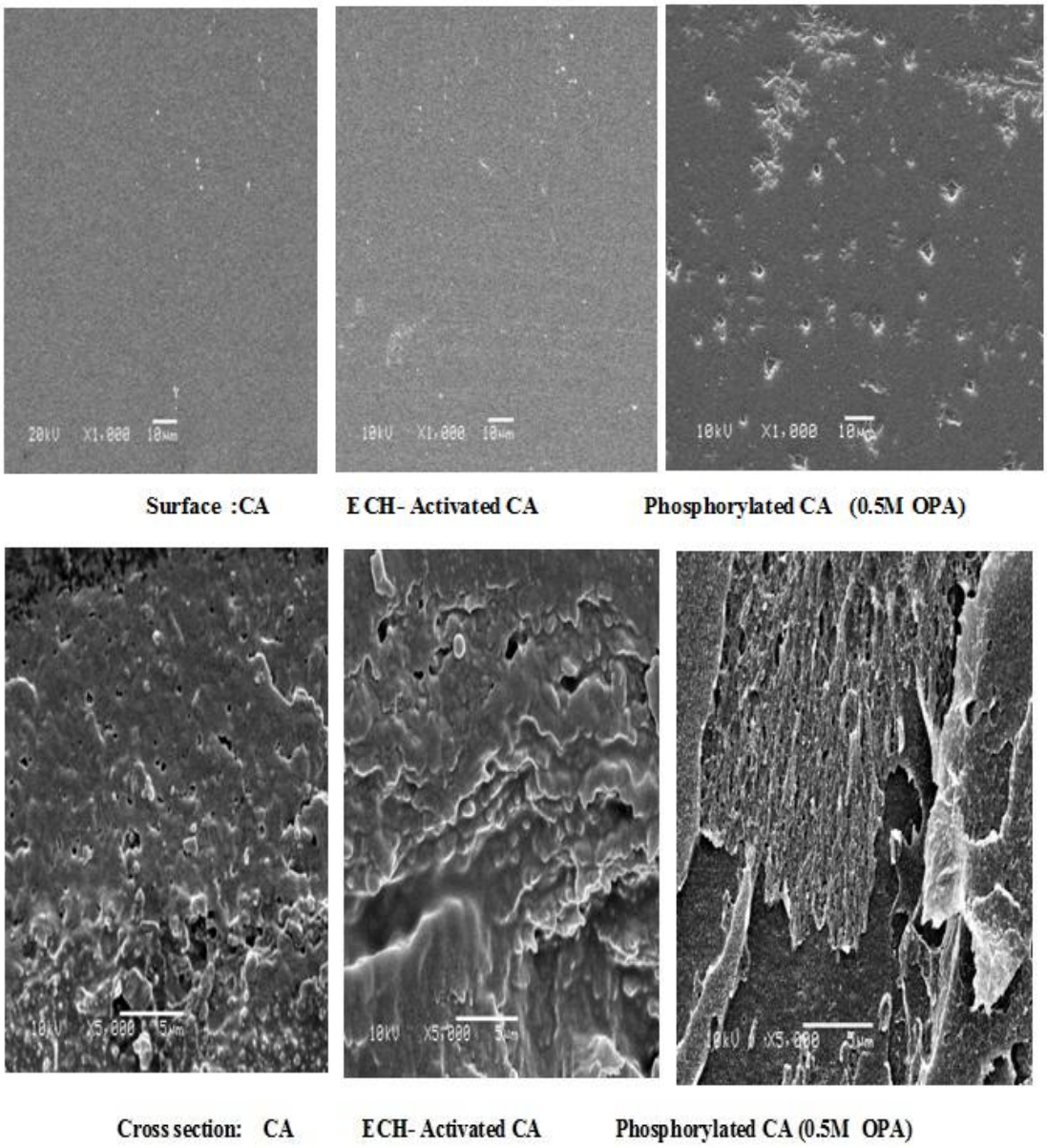

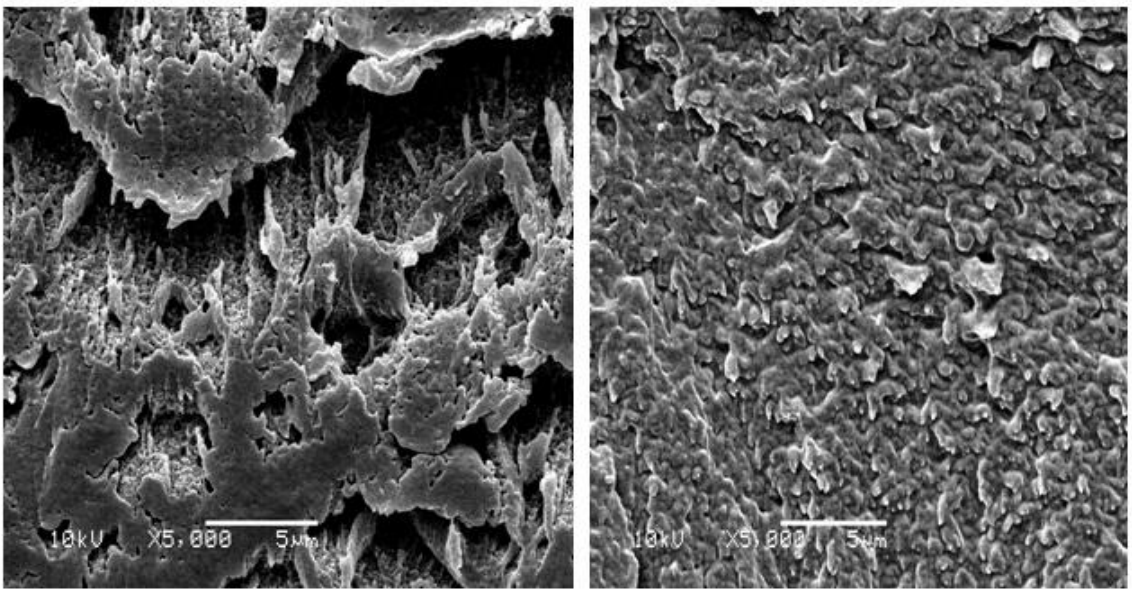

Figure 13. SEM Micrograph of the original CA, activated CA, and phosphorylated CA membranes (surface and cross section).

3.3.7. X-Ray diffraction analysis (XRD)

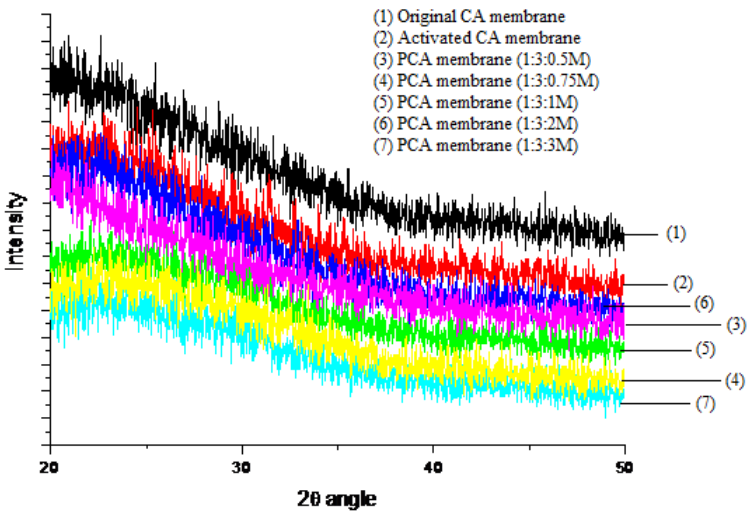

Figure 14. XRD of the original CA, activated CA, and phosphorylated CA membranes.

The x-ray diffraction (XRD) method was used to analyze the original, activated and phosphorylated CA membranes as shown in Figure14.The membranes display a broad diffraction feature at 2θ = 21.295–22.6°, 22.18-22.83°, and 23.16-28.19° for original, activated and phosphorylated CA membranes. Furthermore, the interlayer distances of all membranes calculated from the following equation:

$$2d \sin\theta = n\lambda \quad (8)$$

The data reported as 0.424, 0.4, 0.383 nm for original, activated and (1:3:0.5) phosphorylated CA membranes respectively. This difference in the interlayer space indicates the effect of phosphorization process [42, 43].

3.3.8. Surface roughness test

Surface Roughness variations of the original CA, activated CA and phosphorylated CA membranes shown in Table 4. It was obvious from the results that membranes surface greatly changed by the phosphorization process as the original CA (Ra = 0.05) had a smoother surface than the phosphorylated ones (Ra = 0.522).

Table 4. Surface roughness parameters of phosphorylated CA membranes at different molar ratios of OPA, at 8h and 35°C

CA: ECH: OPA molar ratios	R_a (μm) for the upper surface	R_a (μm) For lower surface
Original CA membrane	0.05	0.08
1: 3: 0.0	0.066	0.064
1: 3: 0.25	0.300	0.522
1: 3: 0.5	0.208	0.137
1: 3: 0.75	0.522	0.148

3.3.9. Optical properties (Color test)

Table 5. Optical parameters of phosphorylated CA membranes at different molar ratios of OPA, at 8h and 35°C

CA: ECH: OPA molar ratios	L*	a*	b*	ΔE*
Original CA membrane	88.04	+0.08	+8.083	49.67
1: 3: 0.0	86.91	+0.07	-8.21	48.88
1: 3: 0.25	87.74	+0.342	-4.913	47.50
1: 3: 0.5	87.86	+0.513	-4.65	48.08
1: 3: 0.75	88.04	+0.350	-5.49	49.83
1: 3: 1	88.85	+0.246	-6.22	49.18

By comparing the optical parameters for the original and activated CA membranes along with the phosphorylated membranes, it is seen in Table 5 that the surface color changes significantly by the phosphorization process.

3.4. Thermal oxidation stability

It was clear from results that the weight of phosphorylated membranes decreases with increasing OPA concentration from 0.25M to 1M under high temperature (up to 80°C) as shown in Figure15.These results may attribute to the hydrophilic nature of the phosphorylated membranes due to the presence of phosphoric groups that are hydrophilic groups.

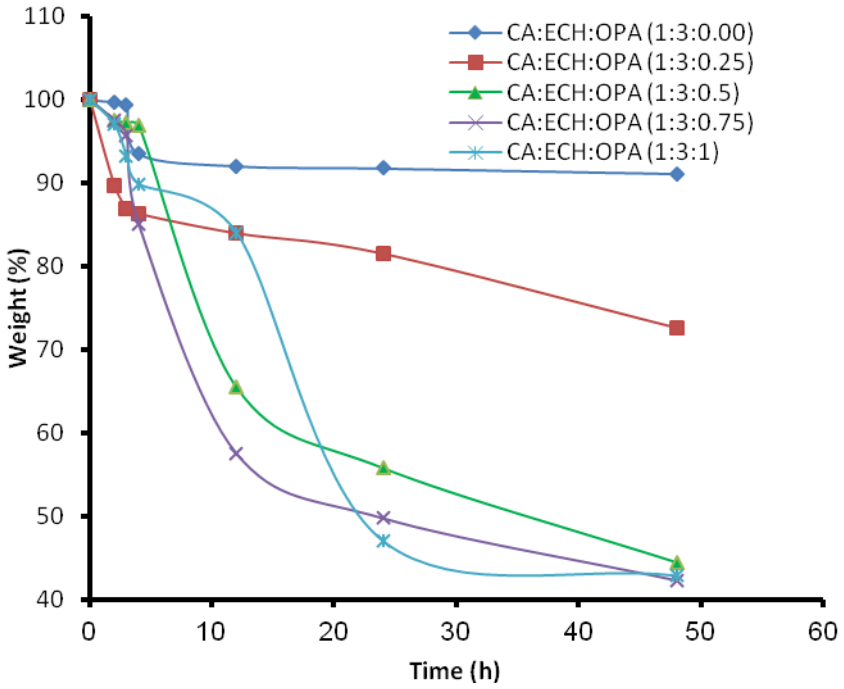

Figure 15. Thermal oxidation stability of the phosphorylated CA membranes with the different molar ratio at 80°C.

3.4.1. Methanol permeability measurements

Also, to having high proton conductivity, the polymer electrolyte membrane of fuel cells is also required effective separation of the fuel and oxidant. Power decrease of the fuel cell results from drawbacks such as transportation of methanol and oxidant gasses across the polyelectrolyte membrane. Efficient fuel cells required highly impermeable methanol polyelectrolyte membranes providing less fuel loss and, as a result, producing higher energy density. In this work, the permeability of methanol for both the Nafion and the phosphorylated membrane with a molar ratio (1:3:0.5 CA: ECH: OPA, respectively) were determined using a diffusion cell in which, the membrane clamped between 2M

methanol in distilled water and distilled water reservoirs. Since the methanol permeable with higher ionic conductivity membranes is the most important feature of fuel cells. HPLC analysis used to follow the concentration of methanol in the water reservoir to estimate the methanol permeability of the optimum membrane under investigation.

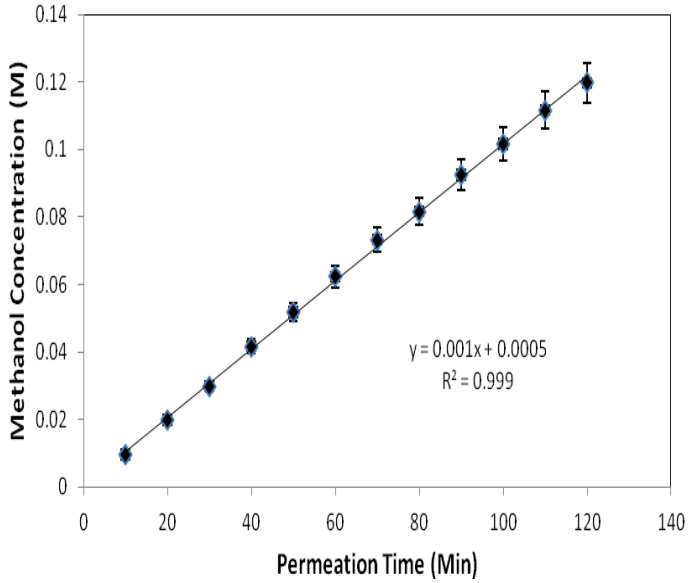

Figure 16. Methanol concentration as a function of permeation time for Nafion 117 membrane **[10]**.

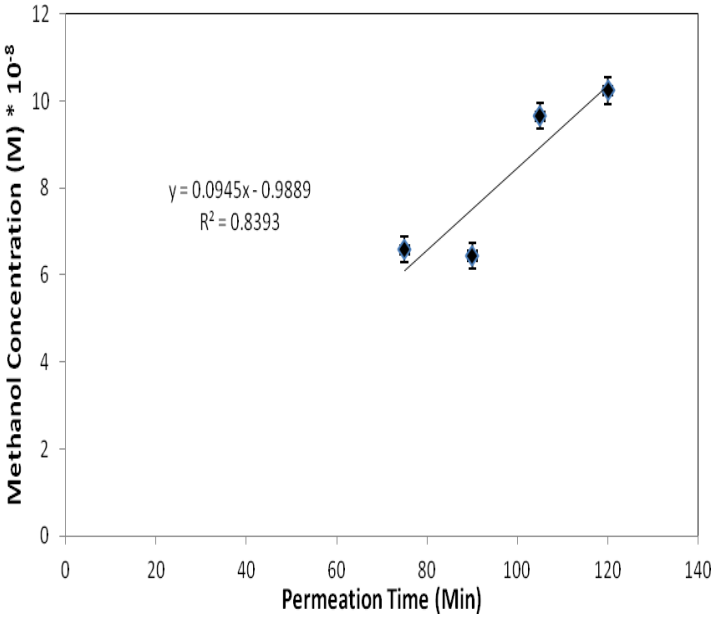

Figure 17. Methanol concentration as a function of permeation time for the phosphorylated membrane.

The change in methanol concentration in the water compartment against the permeation time is represented graphically in Figure 16 and Figure17 for Nafion and phosphorylated membranes respectively. The concentration of methanol in the water compartment is related to the permeation time

according to equation (6). It can observe from Figure 16 and Figure 17 that the methanol concentration in the water compartment for the phosphorylated membrane is lower than that of the Nafion membranes [36]. The slope of the straight line of the change of methanol concentration in the water compartment (C_B) against the permeation time (t) is (α). The methanol permeability *(P)* calculated using equation (7).

$$P = \alpha \frac{V_B}{A} \times \frac{L}{C_A} \qquad (7)$$

Where C_A is the initial concentration of methanol in the compartment (A). A is the membrane working area. L is the membrane thickness. V_B is the volume of water compartment, and *P* is the permeability. It found that the methanol permeability of the phosphorylated membrane ($2.4*10^{-15}$ Cm^2/S) is much lower than that of Nafion®117 membranes ($1.14*10^{-9}$ Cm^2/S).

4. CONCLUSION

Direct methanol fuel cells (DMFCs) present one of the most developing clean energy technologies for portable devices. In this work, a novel phosphorylated cellulose acetate membrane (PCA) designed for the first time. The epoxy groups were introduced firstly through activation step using epichlorohydrin (ECH), followed by phosphorization with orthophosphoric acid (OPA) for inducing the ion exchange capacity (IEC), thermal stability and mechanical properties of CA membranes.Different factors affecting the character of the phosphorylated membranes especially ion exchange capacity (IEC) were optimized and investigated to have the optimum preparation conditions. The chemical structure, thermal stability and morphological structure of the phosphorylated membranes were studied using FTIR, TGA, XRD and SEM analysis techniques. IEC of the prepared membranes obtained in the range 0.4-2meq/g with variation OPA concentration from 0.25M to 2M. PCA membranes show improved mechanical properties. On the other hand, the water uptake of PCA membranes increased from 10.3846% to 18.7648% whereas the methanol uptake reduced from 9.0225% to 4.0723% comparing with native CA membrane.The obtained results revealed that the methanol permeability decreased by 90% regardless to that of the Nafion membrane. Additionally, other physical characterizations such as surface roughness, dimension changes, optical properties, wettability, and thermal oxidation stability were also investigated. The results clearly suggested that the novel PCA membranes could be a suitable polymer electrolyte membrane for DMFCs applications due to the low methanol permeability, the availability and very low price of the CA material compared to the Nafion membranes.

References

1. K. Miyatake, Y. Chikashige, E. Higuchi, M.Watanabe, *JACS* 129 (2007) 3879-3887.
2. C. Bi, H. Zhang, Y. Zhang, X. Zhu, Y. Ma, H. Dai, S. Xiao, *J Power Sources* 184 (2008) 197-203.
3. S. E. Nam, S. O. Kim, Y. Kang, J. W. Lee, K. H. Lee, *J Membrane Sci*., 322 (2008) 466-474.

4. L. Gui, C. Zhang, S. Kang, N. Tan, G. Xiao, D.Yan, *Int. J. Hydrogen Energ.*, 35 (2010) 2436-2445.
5. J. K. Lee, "Direct Methanol Fuel Cell from Polymer Blends", Case Western Reserve University, Department of Chemical Engineering: January, (2006).
6. S. Smith, *Corporate Environmental Strategy*, 6 (1999) 270
7. F. Panik, *J Power Sources*, 71 (1998) 36-38.
8. B. S. Pivovar, Y. Wang, E.L. Cussler, *J Membrane Sci*., 154 (1999) 155-162.
9. C-C. Yang, *Int J Hydrogen energ*., 36 (2011) 4419-4431.
10. A. B. A. Amine, Preparation of Polyelectrolyte Membranes and Electrodes for Direct Methanol Fuel Cells, MSc thesis, FACULTY OF SCIENCE AL-AZHAR UNIVERSITY, CAIRO, 2007.
11. K. A. Mauritz, R. B. Moore, *Chem Rev.,* 104 (2004) 4535-4586.
12. M. A. Hickner, H. Ghassemi, Y. S. Kim, B. R. Einsla, J. E. McGrath, *Chem Rev.*, 104 (2004) 4587-4612.
13. X. Zhu, Y. Liang, H. Pan, X. Jian, Y. Zhang, *J Membrane Sci*., 312 (2008) 59-65.
14. R. Wycisk, J. Chisholm, J. Lee, J. Lin, P. N. Pintauro, *J Power Sources* 163 (2006) 9–17.
15. B. G. Choi, H. Park, H. S. Im, Y. J. Kim, W. H. Hong, *J Membrane Sci*., 324 (2008) 102–110.
16. X. Zhang, S. W. Tay, L. Hong, Z. Liu, *J Membrane Sci*., 320 (2008) 310–318.
17. Y. F. Lin, C. Y. Yen, C. H. Hung, Y. H. Hsiao, C. C. M. Ma, *J Power Sources* 168 (2007) 162–166.
18. L. C. Chen, T. L. Yu, H. L. Lin, S. H. Yeh, *J Membrane Sci*., 307 (2008) 10–20.
19. B. P. Ladewig, R. B. Knott, A. J. Hill, J. D. Riches, J. W. White, D. J. Martin, J.C.D. Da Costa, and G.Q. Lu, *Chem. Mater.,* 19 (2007) 2372–2381.
20. L. Gubler, S.A. Gursel, G.G. Scherer, *Fuel Cells* 5 (2005) 317-335.
21. J. H. Chen, M. Asano, Y. Maekawa, M. Yoshida, *J Membrane Sci*., 277 (2006) 249-257.
22. S. Meenakshi, S. D. Bhat, A. K. Sahu, P. Sridhar, S. Pitchumani, A. K. Shukla, *J Appl Polym Sci.*, 124 (2012) E73–E82.
23. J. Ma, Y. Sahai, *Carbohydr Polym*., 92 (2013) 955–975.
24. Y. S. Ye, J. Rick, B. J. Hwang, *Polymers* 4 (2012) 913–963.
25. H. Vaghari, H. Jafarizadeh-Malmiri, A. Berenjian, N. Anarjan, *Sustainable Chemical Processes* 1 (2013) 1-16.
26. N. Shaari, S.K. Kamarudin, *J Power Source* 289 (2015) 71–80.
27. P-C Li, G–M Liao, S. R. Kumar, C-M Shih, C-C Yang, D-M Wang, S. J. Lue, *Electrochimica Acta,* 187 (2016) 616-628.
28. T. Malutan, R. Nicu, V. I. Popa, *Bioresources* 3 (2008) 1371-1376,.
29. C. Yang, W. Chien, Y. J. Li, *Int J Hydrogen Energ*., 36 (2010) 3407- 3415.
30. C. Tseng, Y.Ye, K. Kao, J. Joseph, W. Shen, J. Rick, B. Hwang, *Int J Hydrogen Energ*., 36 (2011) 11936-11945.
31. R. Wycisk, W. M. Trochimczuk, *J Appl Polym Sc*i., 43 (1991) 1727-1735.
32. A. Panchenko, H. Dilger, E. Möller, T. Sixt, E.Roduner, *J Power Sources* 127 (2004) 325–330.
33. P. Xing, G. P. Robertson, M. D. Guiver, S. D. Mikhailenko, K. Wang, S. Kaliaguine, *J Membrane Sci*., 229 (2004) 95-106.
34. M. S. Mohy Eldin, E. A. Soliman, E. A. Hassan, M. A. Abu-Saied, *J Appl Polym Sci*., 111 (2009) 2647-2656.
35. M. S. Mohy Eldin, A. A. Elzatahry, K. M. El-Khatib, E. A. Hassan, M. M. El-Sabbah, M. A. Abu-Saied, *J Appl Polym Sci*., 119 (2011) 120-133.
36. W.A. Zisman, Ind. Eng. Chem. 55 (1963) 18-38.
37. N. I. El-Awady, M. M. El-Awady, M. S. Mohy Eldin, *Egy J Polym Sci Technol*., 3 (1999) 25-41.
38. M. S. Mohy Eldin, M. A. Abu-Saied, A. A. Elzatahry, K. M. El-Khatib, E. A. Hassan, M. M. El-Sabbah, *Int J Electrochem Sci*., 6 (2011) 5417-5429.
39. T.A. Zawodzinski, C. Derouin, S. Radzinski, S R.J. Herman, V. T. Smith, T. E. Springer, S. Gottesfeld, *J Electrochem Soc*., 140 (1993) 1041-1047.

40. N. D. Thanh, D. T. Tuyen, "Some Derivatives of Cellulose with Diethanolamine and Ethylenediamine", Faculty of Chemistry, Hanoi University of Science, VNU,19 Le Thanh Tong, Hanoi, Vietnam, (2009).
41. M. H.Woo, O. Kwon, S. H. Choi, M. Z. Hong, H. W. Ha, K. Kim, *Electrochimica Acta*, 51 (2006) 6051–6059.
42. D. Xing, G. He, Z. Hou, P. Ming, S. Song, *Int J Hydrogen Energ*., 36 (2011) 2177-2183.